ARTICLE　　OPEN

Check for updates

Imaging the formation and surface phase separation of the *CE* phase

Haibiao Zhou [1,2,6✉], Qiyuan Feng[1,2], Yubin Hou[1], Masao Nakamura [3], Yoshinori Tokura [3,4], Masashi Kawasaki[3,4], Zhigao Sheng [1,2,5✉] and Qingyou Lu [1,2,5✉]

The *CE* phase is an extraordinary phase exhibiting the simultaneous spin, charge, and orbital ordering due to strong electron correlation. It is an ideal platform to investigate the role of the multiple orderings in the phase transitions and discover emergent properties. Here, we use a cryogenic high-field magnetic force microscope to image the phase transitions and properties of the *CE* phase in a $Pr_{0.5}Ca_{0.5}MnO_3$ thin film. In a high magnetic field, we observed a clear suppression of magnetic susceptibility at the charge-ordering insulator transition temperature (T_{COI}), whereas, at the Néel temperature (T_N), no significant change is observed. This observation favors the scenario of strong antiferromagnetic correlation developed below T_{COI} but raises questions about the Zener polaron paramagnetic phase picture. Besides, we discoverd a phase-separated surface state in the *CE* phase regime. Ferromagnetic phase domains residing at the surface already exist in zero magnetic field and show ultra-high magnetic anisotropy. Our results provide microscopic insights into the unconventional spin- and charge-ordering transitions and revealed essential attributes of the *CE* phase, highlighting unusual behaviors when multiple electronic orderings are involved.

INTRODUCTION

Strong electron correlation in materials usually leads to complex and emergent phenomena[1], which provide a fertile ground for exploring new physics and hold great potential for applications. The colossal magnetoresistance in perovskite manganites and unconventional high-T_C superconductivity in cuprates are the two most distinguished phenomena in strongly correlated oxides. These materials share many common characteristics. For example, both of them exhibit a variety of phases with contrasting properties. In manganites, there exist the well-known ferromagnetic metallic (FM) phase, antiferromagnetic (AFM) charge-ordered insulating (COI) phase, and so on. Among them, the *CE* phase, first proposed by Goodenough in the 1950s[2], is most prominent as it is an exceptional realization of simultaneous ordering of spin, charge, and orbital. How the phase transitions and properties are affected in the presence of multiple orderings is a pivotal question in strongly correlated materials. Hence, the *CE* phase, existing in narrow-bandwidth half-doped manganites, such as $RE_{0.5}Ca_{0.5}MnO_3$ ($RE =$ Pr, Sm, Y, Nd, etc)[3–7] and single-layered manganite $La_{0.5}Sr_{1.5}MnO_4$[8], is an ideal platform to investigate these effects[9].

These half-doped manganites show a similar phase diagram as in Fig. 1a, which is for bulk $Pr_{1-x}Ca_xMnO_3$[3,4]. When close to half doping ($x \sim 0.5$), before entering the *CE* phase, it first undergoes a transition from paramagnetic (PM) phase to charge/orbital-ordered insulating phase at a charge-ordering insulator transition temperature (T_{COI}) = 240 K, then followed by an AFM transition at Néel temperature (T_N) = 175 K. Below T_N it shows the *CE*-type charge, spin and orbital ordering (Fig. 1b)[2]. This *CE* phase features the ferromagnetic zigzag chains consisting of Mn^{3+}/Mn^{4+} ions with alternating $d_{3x^2-r^2}$ and $d_{3y^2-r^2}$ orbitals at the Mn^{3+} ion sites,

driven by the competition between the electron kinetic energy and magnetic exchange energy[10,11]. Besides, it has an equal number of Mn^{3+} and Mn^{4+} cations, resulting in a concomitant charge ordering with a checkboard pattern. Owing to the enhanced tendency towards the COI state at this doping level, the *CE* phase possesses a high melting magnetic field and shows the largest colossal magnetoresistive effect. For example, a magnetic field larger than 30 T is needed to transform this phase into the FM phase in bulk $Pr_{0.5}Ca_{0.5}MnO_3$[12], which is, however, inaccessible to most investigating tools.

Although this phase has attracted intensive interest, several mysteries remain to be fully solved. A thorough investigation of these questions is crucial to our understanding of strongly correlated systems. One of them is how the *CE* phase is formed. Unlike many other manganites where spin and charge orderings occur at the same temperature, the *CE* phase is attained after the successive COI and AFM transitions. But, the drop of magnetization, expected to occur at T_N, appears at T_{COI} instead. Although at T_N, no well-defined signal has been detected (Fig. 1c). The nature of the magnetic anomaly at T_{COI}, as well as the magnetic structure of the intermediate phase between T_{COI} and T_N, has been a long-lasting puzzle. This is common to the aforementioned half-doped manganites. At present, there are mainly two scenarios proposed for this discrepancy. In the one model, which we call short-range AFM correlation scenario, the decrease in magnetization at T_{COI} has been attributed to the quenching of double-exchange interaction and onset of AFM correlation, due to the localization of the charge carriers[8,13–15]. Short-range antiferromagnetically coupled zigzag chain fragments start to form at this temperature, and the smooth increase of magnetic correlation across T_N is ascribed to the coherent ordering of the zigzag chains[15]. However, the evidence

[1]Anhui Key Laboratory of Condensed Matter Physics at Extreme Conditions, High Magnetic Field Laboratory, HFIPS, Anhui, Chinese Academy of Sciences, Hefei, China. [2]Hefei National Laboratory for Physical Sciences at the Microscale and Anhui Laboratory of Advanced Photon Science and Technology, University of Science and Technology of China, Hefei, China. [3]RIKEN Center for Emergent Matter Science (CEMS), Wako, Saitama, Japan. [4]Department of Applied Physics and Quantum Phase Electronics Research Center (QPEC), University of Tokyo, Tokyo, Japan. [5]Collaborative Innovation Center of Advanced Microstructures, Nanjing University, Nanjing, China. [6]Present address: Department of Condensed Matter Physics, Weizmann Institute of Science, Rehovot, Israel. ✉email: haibiaozhou24@gmail.com; zhigaosheng@hmfl.ac.cn; qxl@ustc.edu.cn
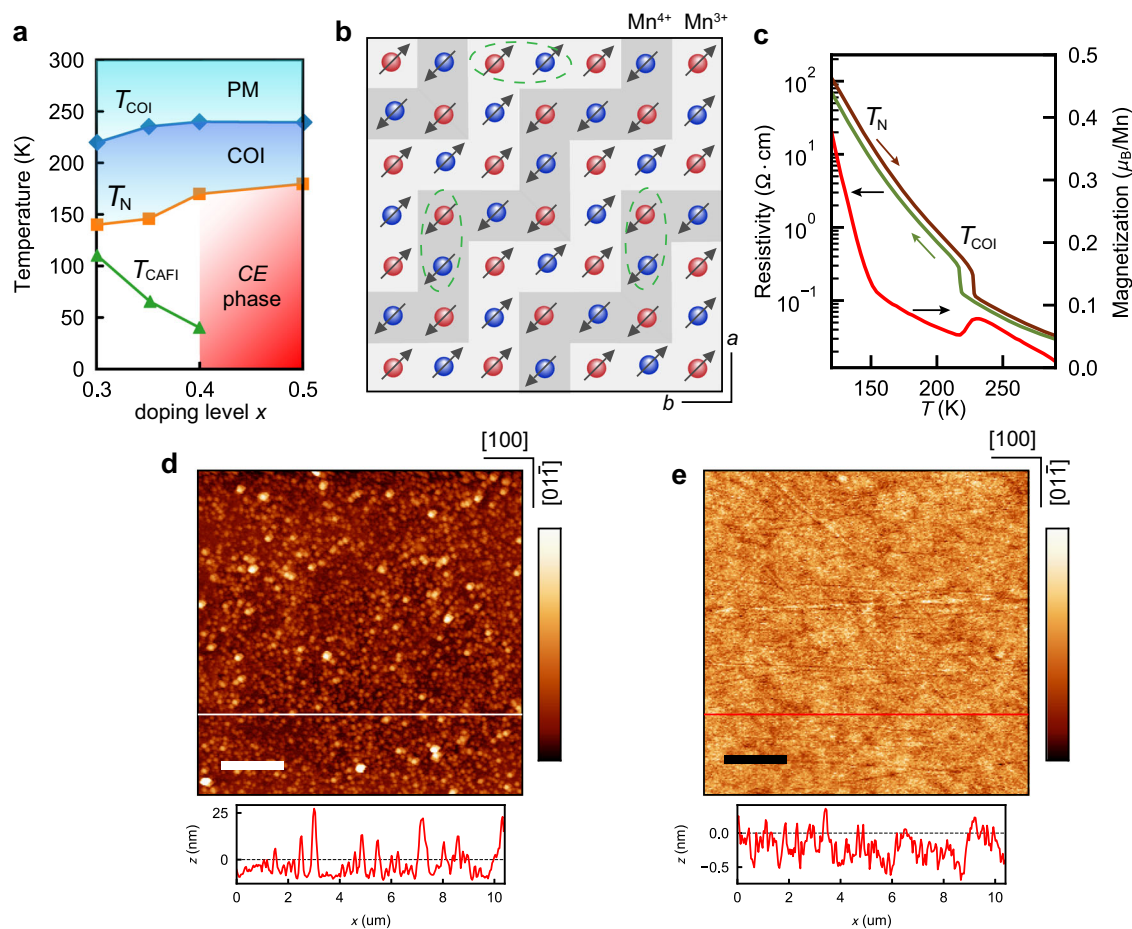
Fig. 1 Phase diagram, electrical, and magnetic properties of PCMO. a Phase diagram of $Pr_{1-x}Ca_xMnO_3$ as a function of the doping level x adapted from ref. [4]. PM, COI, and CAFI denote the paramagnetic insulator, charge-ordered insulator, and canted antiferromagnetic insulator phase, respectively. **b** Schematic illustration of the charge and spin ordering in the *CE* phase. The ferromagnetic zigzag chains are shown by the gray and light gray zigzag regions. The green-dashed ovals indicate the Zener polarons. **c** The temperature dependence of the resistivity and magnetization of the imaged PCMO film. The resistivity was measured in zero field and the magnetization was measured in 0.1 T applied along [100] axis with the diamagnetic response of the substrate subtracted. **d–e** Rough and flat topography observed in this film at different locations. Image size: $10.4 \times 10.4 \ \mu m^2$. Scale bar in **d** and **e**: 2 μm. Color scale: 60 nm (**d**) and 2.2 nm (**e**).

Table 1. Qualitative comparison between different scenarios and measured MFM contrast.

T	H	Conventional AFM transition		Zener polaron scenario		Short-range AFM correlation scenario		Measured contrast
		Spin alignment	Contrast	Spin alignment	Contrast	Spin alignment	Contrast	
T_{COI}	0		None		None		None	
	Low		None		Weak		Weak	Weak
	High		None		Weak		Strong	Strong
T_N	High		Strong		Strong		None/weak	None

The rectangular regions, filled with arrows and different colors represent the different phases. The gray, red, orange, and green regions are the paramagnetic, *CE*, Zener polaron PM, and short-range AFM-correlated phases, respectively.

has been very limited to neutron scattering experiments[14,15]. The other one which is based on the formation of Zener polarons (ZP) has also gained much support after the seminal work of Daoud-Aladine et al.[5,16–18]. In contrast to the ideal site-centered checkboard pattern expected in the *CE* model, in this picture, the ferromagnetic Mn^{3+}-Mn^{4+} dimers, so-called ZP, start to form at T_{COI} mediated by the oxygen atom (Fig. 1b), resulting in a PM

phase consisting of ZP below T_{COI}. Suppression of the magnetization is then expected as a consequence of the paring of Mn–Mn ions. The magnetic moments are doubled in magnitude but halved in number in the ZP PM phase[5]. The associated ferroelectric ordering due to inversion symmetry breaking has been reported in various manganites later[16,17,19–21]. It is worth noting that though it is highly demanding, no real-space microscopic imaging results
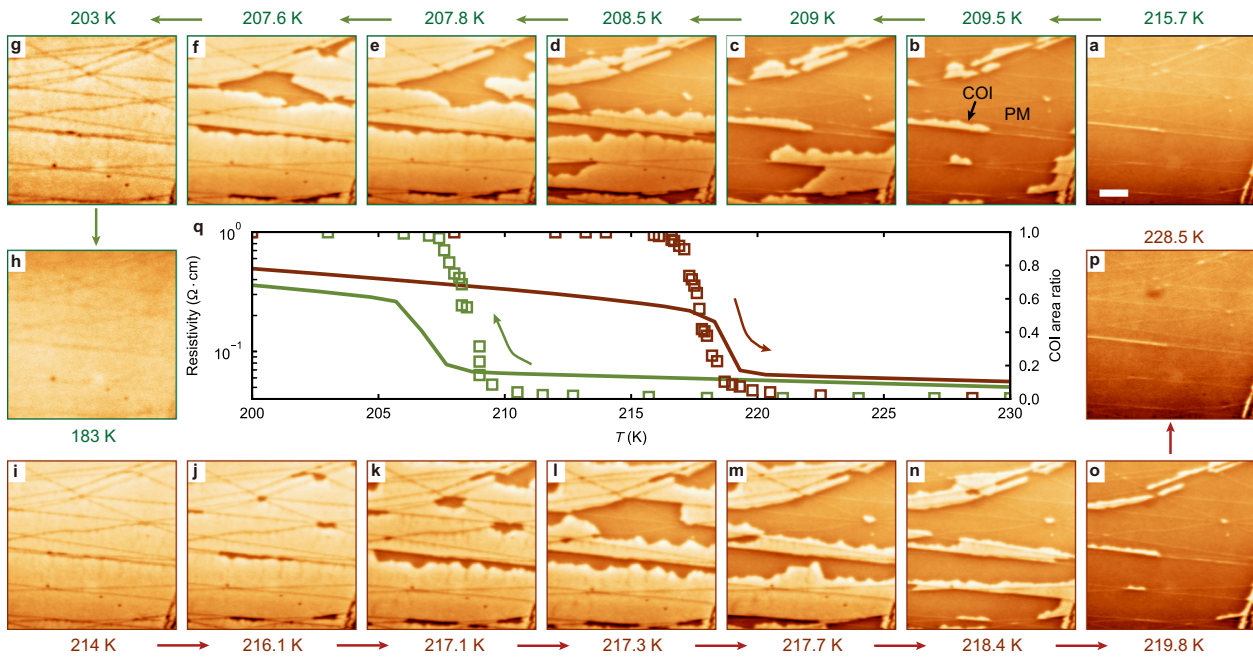
Fig. 2 Imaging the magnetic contrast at T_{COI}. The magnetic images are taken on a rough region while the sample is cooled down from room temperature to 183 K (**a–h**) and then warmed up to 230 K (**i–p**) in a field of 9 T. The arrows indicate the imaging sequence. **q** shows the temperature dependence of resistivity in 9 T (solid lines) and the area ratio of the charge-ordering insulating (COI) phase (open squares) extracted from the MFM images. Scale bar in **a**: 2 μm. MFM image size: 11.8 × 11.8 μm². The contrast is ~0.5 Hz for all the images.

have been reported so far for the transitions at T_{COI} and T_N, mainly limited by the required high magnetic field. Microscopic evidence would be highly beneficial to this debate[22–28] and also the ongoing controversy of site-centered or bond-centered charge ordering in transition metal oxides[25,29,30]. In this work, we show that it is possible to distinguish these scenarios through magnetic imaging in high magnetic fields, as they would give rise to very different magnetic contrasts.

Another intriguing phenomenon is the variation of the *CE*-type ordering when the size or dimension of the sample is reduced. Magnetic hysteresis has been widely observed in half-doped manganite nanoparticles[31] and nanowires[32], which is evidence of an FM phase or superparamagnetic phase. Motivated by this, the polar surfaces of half-doped manganites in the *CE* phase regime have been predicted to possess a unique state, arising from a deviating charge density ($n_e = 0.75$) at the surface layer from half doping. It is neither a pure COI phase nor an entire FM phase. Rather, it is a PS state, i.e., a coexistence of the two phases at the surface[33]. This PS surface state in the *CE* phase regime, however, still lacks direct evidence. Interestingly, an AFM state at the surface of FM manganites has been observed, which is attributed to the enhanced spin-orbit coupling at the surface[34]. More generally, it is still an open question whether there exists a bulk-surface correspondence in the magnetic or electronic states in strongly correlated systems. Hence, it is of crucial importance to verify this prediction and further reveal the surface characteristics, and magnetic imaging has been demonstrated as an ideal tool to study magnetic phase separation.

In this article, we report the real-space magnetic imaging of the magnetic transitions at T_{COI} and T_N, and the *CE* phase in a Pr$_{0.5}$Ca$_{0.5}$MnO$_3$ (PCMO) thin film. The 30-nm thick PCMO thin film was grown on a (LaAlO$_3$)$_{0.3}$(SrAl$_{0.5}$Ta$_{0.5}$O$_3$)$_{0.7}$ (LSAT) (011) substrate using pulsed laser deposition (see Methods). The PCMO/LSAT (011) film (in pseudocubic notation) shows similar charge, orbital, and magnetic transitions with the bulk sample, but with reduced transition temperatures ($T_{COI} = 210$ K and $T_N = 150$ K)[35,36] and melting field[37]. The magnetic force microscope (MFM) equipped with a 20 T superconducting magnet used in this work has been

described in detail elsewhere[38,39]. In brief, the contrast in MFM images comes from the long-range magnetic force between the sample and the magnetic tip. We emphasize that in the present work, the accessible high magnetic field brings us manifold advantages. First, owing to the enhanced contrast in high magnetic fields, one is capable of imaging the magnetic susceptibility change even when only weakly magnetic phases are involved[40], which is crucial for the present work. Second, in high fields, very different contrast is expected for the two scenarios proposed for the magnetic anomaly at T_{COI}, which can be directly compared with the collected MFM images. Third, this will enable us to reveal some important high-field features of the surface magnetic structures.

RESULTS AND DISCUSSION

Magnetic images at T_{COI} and T_N

Before presenting the magnetic images, we summarize in Table 1 the image contrasts expected for a conventional PM to AFM transition and the cases of the above two scenarios. Generally, both PM and AFM phase shows zero net magnetic moments in zero field, but PM phase will show large magnetization in a strong magnetic field. Hence, in the case of a conventional PM to AFM phase transition, one should only see the image contrast during the phase domain formation in a high magnetic field at T_N, but not at T_{COI}. In the ZP picture, one should be able to see a reduced susceptibility at T_{COI} as the ZP PM phase has slightly smaller susceptibility[5], but a much larger contrast at T_N should also be observed when it enters the AFM phase in a high field. However, in the short-range AFM correlation picture, short-range AFM domains start to form at T_{COI}, and one would be able to see an obvious domain formation at T_{COI}, whereas at T_N there should be little or no change depending on whether we can see the domain walls between the short-range zigzag chains. The strikingly different contrasts under high magnetic fields for these pictures highlight the advantage of high-field magnetic imaging. In principle, macroscopic magnetization measurements should also be able to reveal these differences. However, these measurements (including Fig. 1c) usually see a PM behavior even below T_N, which
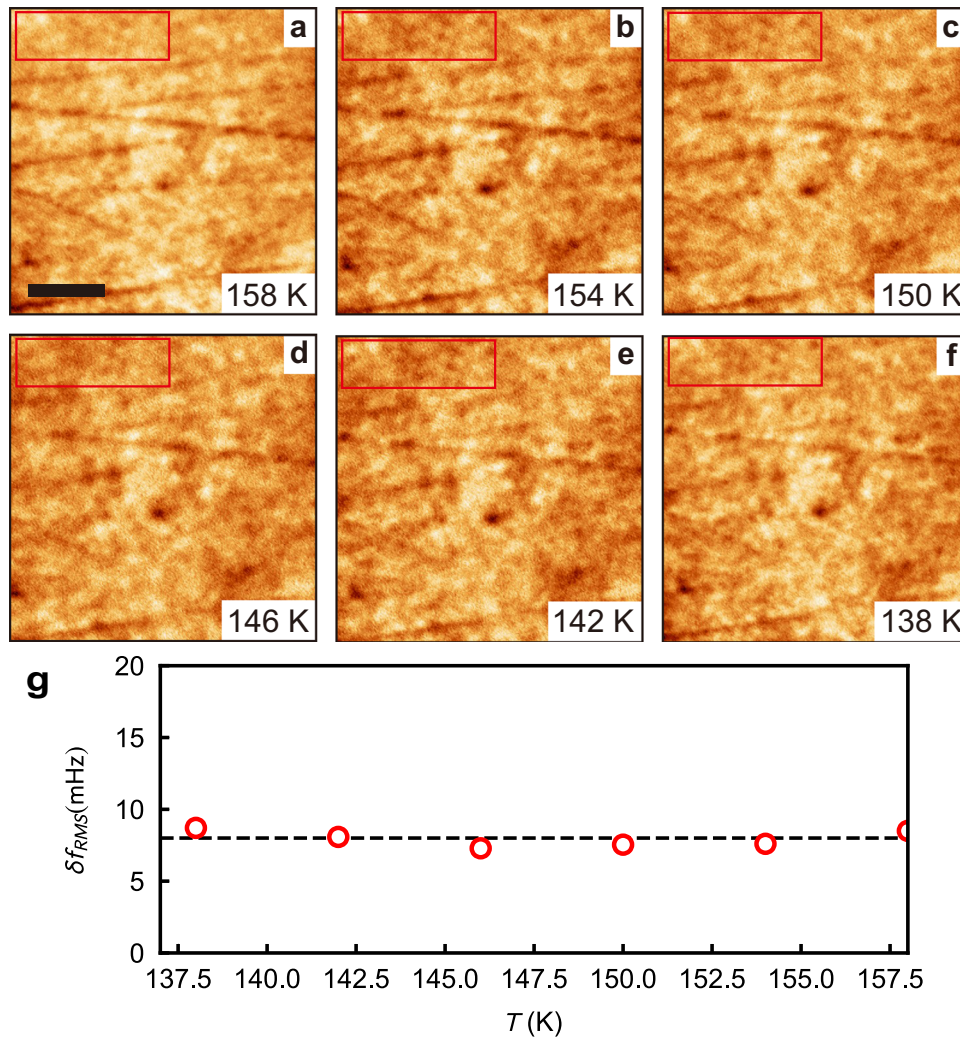
Fig. 3 Absence of significant change when the sample is cooled down through T_N. a–f MFM images taken on a rough region while the film is field-cooled through $T_N = 150$ K from room temperature in 9 T. Scale bar in **a**: 1 μm. Image size: 4×4 μm². **g** The root-mean-square (RMS) of the magnetic contrast in the region marked by the dashed red rectangle in the images of **a**. The color scale is 75 mHz for all the MFM images.

is generally ascribed to impurities[5,11,15,36]. Local magnetic imaging microscopy would spare us their contribution.

We observed two types of surface on this single PCMO film with MFM: one is rough and covered with nanosized particles (Fig. 1d), which might be MnO_x, whereas the other one is very flat but shows several crosshatching lines (Fig. 1e), similar to other manganite films owing to the presence of epitaxial strain[41]. It will be shown that the crosshatching lines are also present underneath those particles on the rough region. These lines act as the nucleation sites of the phase domains. The root-mean-square roughness of the two-type surfaces is ~10 nm and 3.5 Å, respectively. The reason for the formation of two types of surface is unclear yet.

In Figs. 2 and 3, we show the MFM images of the sample when it is cooled down in 9 T field through T_{COI} and T_N, respectively. At 215.7 K, some bright stripes residing close to the crosshatching lines are readily observed. As the temperature is going down, these stripes expand and gradually occupy the imaged area (183 K). Then when the sample is warmed up, the phase with darker contrast nucleates and expands, with the brighter phase domains shrinking towards the line defects. The dark phase domains dominate the sample at above 219 K. The hysteresis undoubtedly indicates it is a first-order phase transition, and the temperature dependence of the area portion of the bright regions matches very well with that of the measured resistance. Thus, the

dark and white regions are ascribed to the PM and COI phases, respectively. The brighter contrast of the COI phase suggests it has a smaller attractive force with the magnetic tip, thus a weaker magnetic susceptibility than the PM phase. The image contrast is greatly enhanced in 9 T compared with 0.5 T (Supplementary Figure 1). When the sample is cooled through T_N, no noticeable change is observed in the MFM images (Fig. 3 and Supplementary Figure 2). Note that the imaged area has a rough surface.

Hence, these images can be well explained by the short-range AFM correlation scenario (Table 1). In these half-doped manganites, there exist the competing FM correlation and CE-type AFM correlation. At T_{COI}, electron localization suppresses the double-exchange FM interaction, whereas enhances the CE-type AFM correlation[8,13,15]. Short-range zigzag chains that are antiferromagnetically coupled start to form at T_{COI}, as revealed by previous neutron scattering experiments performed in the nearly half-doped $Pr_{0.55}(Ca_{0.8}Sr_{0.2})_{0.45}MnO_3$[14], and half-doped single-layer manganite $La_{0.5}Sr_{1.5}MnO_4$[15,25]. This causes the susceptibility drop seen in the macroscopic magnetization and MFM images. The AFM correlation length increases gradually when the sample enters the CE phase, suggesting the short-range chain fragments merge into larger domains when the temperature is lowered[14,15]. The fact that the spin ordering nucleates at T_{COI}, but its coherent ordering occurs only at T_N, implies unconventional phase dynamics[14,42], perhaps a unique
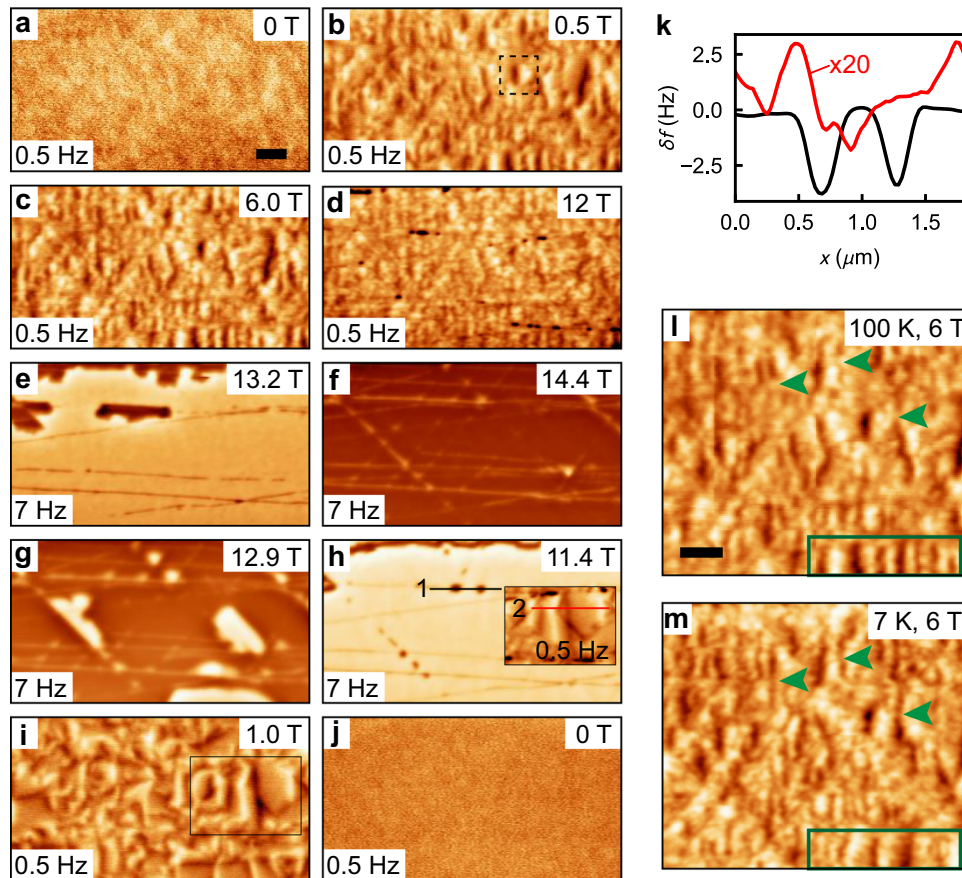
Fig. 4 Magnetic images of surface phase separation. a–j MFM images taken on a flat region in different magnetic fields at 100 K, with the color scales labeled. The dashed rectangle in **b** contains a pair of dark and bright contrast. The inset in **h** shows the area with a reduced color scale (0.5 Hz) to highlight the weakly magnetic features. Scale bar in **a**: 1 μm. Image size: 11×6 μm^2. **k** The line profiles taken along the two lines marked in **h**. The data for the red line is multiplied by a factor of 20. **l–m** A zoom-in view of the patterns after the sample is cooled down to 100 K (**l**) and 7 K (**m**) in different thermal cycles. Scale bar in **l**: 1 μm. Image size: 7×6 μm^2. A magnetic field of 6 T is later applied to enhance the contrast. The arrows and frames indicate the changes of the domains.

feature of the *CE*-type ordering[15]. However, we do not observe the evolution of the short-range domains between T_{COI} and T_N, implying the COI phase domains are all occupied with the short-range zigzag chain segments and the separation between the domains is smaller than the MFM spatial resolution (~30 nm). It is worth noting that the suppression of magnetic susceptibility is also observed at the charge-ordering transition temperature in some other non-half-doped manganites $Bi_{0.18}Ca_{0.82}MnO_3$[43] and some nickelates[44], which may also be driven by a similar mechanism. That said, our results would also be consistent with the Zener polaron picture, as long as the strong AFM correlation of the ZP is also involved.

Phase-separated surface state in the *CE* phase regime

We indeed see some prominent changes on the flat region when the sample enters the *CE* phase at T_N (Supplementary Figure 3). We imaged the formation of some local FM features. Nevertheless, these features are not related to the field-induced COI to FM transition as they are already present in zero field[37].

To show more details of the local FM structures, in Fig. 4, we present a series of MFM images taken in a magnetic field swept between 0 and 14.4 T at 100 K after the sample is cooled down in zero field. The zero-field image already shows some faint mist-like contrast, which is significantly enhanced by the application of 0.5 T field, where fine stripe-like features elongated along the vertical direction ([01-1] axis) are observed. A pair of bright and dark regions as indicated by a dashed line box evidences an in-plane magnetic easy axis. However, these features show little

change as we increase the magnetic field except that the magnitude of contrast is enhanced, even until the *CE* phase starts to melt, as seen when the large FM domains appear (Fig. 4e). When the magnetic field is ramped down, the *CE* phase reappears (Fig. 4g). Interestingly, there also exist such FM features inside the *CE* phase domains, which are highlighted with a reduced color scale in the rectangular region in Fig. 4h. The domain pattern is now less anisotropic, with a shape strongly different from the case before the *CE* phase is melted (see Fig. 4e and Supplementary Figure 4). The pattern does not change when the magnetic field is further decreased (Fig. 4i), suggesting they are also pinned, similar to the field sweep-up process. In Fig. 4l–m, the images taken at 7 K and 100 K for two different thermal cycles are shown. The patterns are almost the same, and one can readily see how the small domains merge when the temperature is lowered.

We argue that the observations fully agree with the aforementioned numerical simulations based on the two-orbital double-exchange model when taking into account the polar surface of $Pr_{0.5}Ca_{0.5}MnO_3$[33]. First, the magnetic domains appear at ~150 K, suggesting that it is related to the AFM transition and *CE* phase. Second, the fact that the FM phase domains are much more evident on the flat region implies that it is related to the surface (Supplementary Figure 5). Third, the magnetic contrast of these features is ~20 times smaller than that between the COI and FM phases (Fig. 4l), indicating they are due to some magnetic structures that are not homogeneous through the whole film thickness. In addition, as all the low-field FM domains possess a
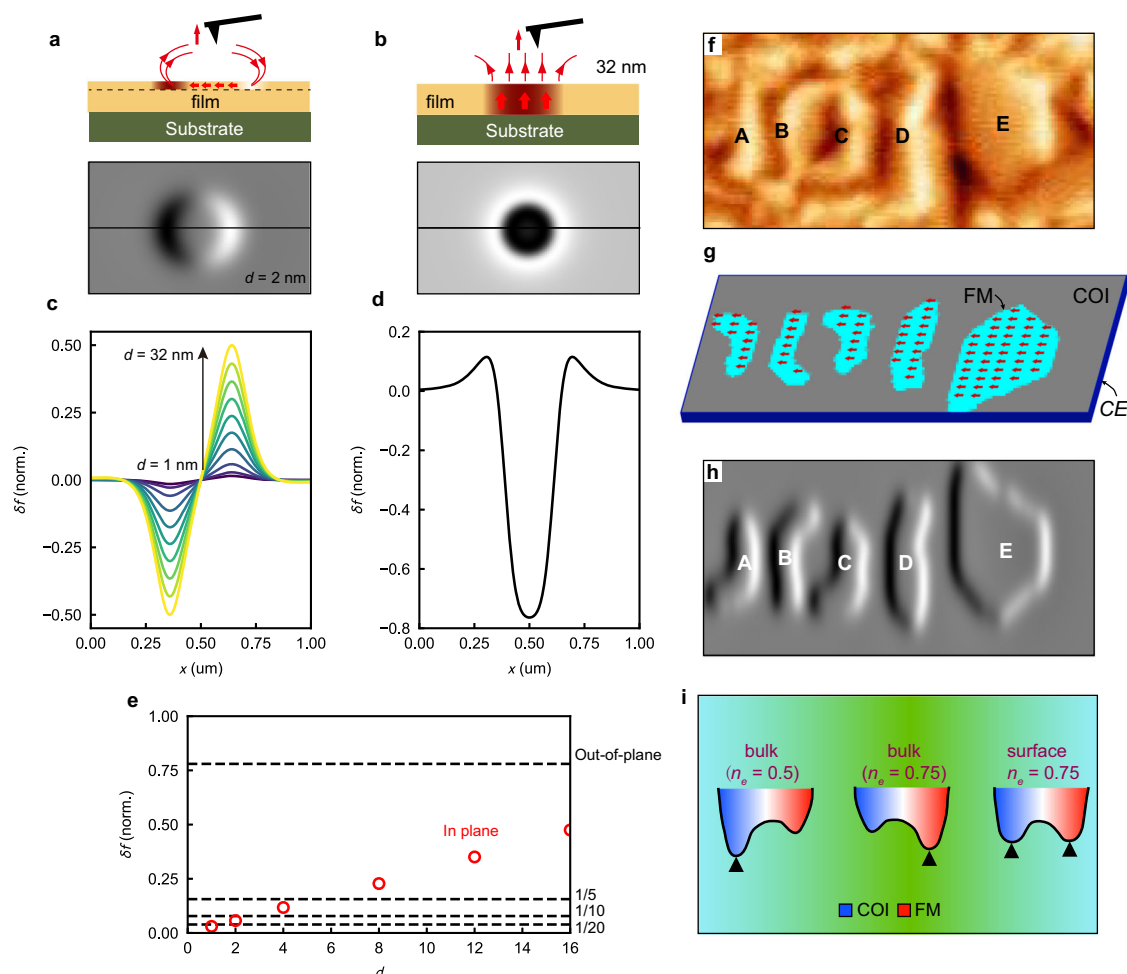
Fig. 5 Simulation of the magnetic images. a–b Simulated magnetic images of in-plane and out-of-plane magnetic domains. Size of simulated image: $1 \times 0.6 \, \mu m^2$. The domain with 2 nm thickness is shown in **a**. Both domains have a diameter of 300 nm. **c** The thickness dependence of the profiles along the horizontal line across the center of domains. **d** Profile along the line in **b**. All the profiles in **c** and **d** are normalized by the same factor. **e** The thickness dependence of the contrast magnitude of in-plane magnetic domains (red open circles). The dashed line is the contrast of out-of-plane magnetic domains divided by a factor of 1, 5, 10, and 20. **f** A zoom-in of the surface phase separation pattern. Several large FM phase domains are marked with **A**, **B**, **C**, **D**, and **E**. **g** Illustration of the net magnetic moments at the surface. **h** Simulated MFM image of FM phase domains (**A**–**E**) based on the magnetic moment distribution shown in **g**. **i** Schematic showing how the ground state changes with the charge density and surface.

similar magnetic contrast and orient along the same direction, it is highly unlikely that they reside at different layers of the film or have different environments.

Hence, it is likely that they are local ferromagnetic domains located at the surface with similar thickness, which is illustrated in Fig. 5a. To deduce the thickness of the FM domains from the MFM images, we simulate the contrast of in-plane domains (Fig. 5a) residing at the surface as a function of its thickness and that of out-of-plane domains (Fig. 5b) through the whole film thickness. The magnetic signal shows an almost linear dependence on the number of layers (Fig. 5c–e). Using the magnitude ratio ~20 extracted from the experiment (Fig. 4k) yields a thickness of ~1 nm (approximately four layers of MnO planes in the [011] direction) for the in-plane magnetic moments (Fig. 5e). With this thickness and a speculated distribution of the magnetic moments at the surface as in Fig. 5g, we can then simulate the magnetic image of the several large FM phase domains in Fig. 5f, h.

Though in the original simulation in ref. [33], the simplest (001) terminated surface is considered, the results can in principle be extended to other polar terminations, including the current case, (011) termination. It is worth emphasizing that, the interior of the film at this doping level ($n_e = 0.75$) would show an FM phase.

Hence, the surface PS is not driven by the charge density deviation. It is the surface with inversion symmetry breaking that alters the free energy landscape, which eventually leads to the phase-separated state (Fig. 5i). The suppression of AFM super-exchange interaction or electron–phonon interaction at the surface is likely to be the reason[33]. It remains to be explored whether other surfaces of PCMO, as well as other narrow-bandwidth half-doped manganites, show similar properties. Also, the detailed structure of the film surface needs to be confirmed. For instance, the model assumes that the surface has intact oxygen octahedra and no defects, but the real surface structure of (011) termination should be more complicated. The influence of defects at the surface, which would change the charge density, also needs to be taken into account.

Below we summarize the unique features of the surface PS compared with the conventional PS in the bulk of other manganites: (1) even though both surface and bulk PS are a consequence of competing interactions with similar energies, surface PS arises in the system with the strongest AFM correlation, and it is only present when the bulk is in the CE phase. (2) The FM phase domains show much higher anisotropy than the bulk domains. The magnetic moments remain in the in-plane direction

([100] axis) even in a field of 12 T. As far as we know, this is the largest known anisotropy. It probably originates from the super-exchange interaction between magnetic moments in the surface FM phase and bulk *CE* phase[45], which would also result in an enhancement of exchange bias[46,47]. This suggests a route of achieving high magnetic anisotropy through the pinning effect in PS systems. (3) The vastly different patterns seen after a field-sweep cycle indicate the magnetic domains are not due to static impurities or strain. However, these domains are pinned in different thermal cycles. This pinning effect, which is only observed in thermal cycles, remains unclear.

Nevertheless, they share some common features. The textures of the surface PS do not change with the magnetic field until the COI phase domains are melted[39], which is similar to other PS systems[39,48]. The COI phase domains at the surface have a similar melting magnetic field as the bulk of the film.

To conclude, we revealed how the *CE* phase is developed and its surface state in a PCMO thin film through high-field magnetic imaging. The real-space microscopic images clearly show a large suppression of the local magnetic susceptibility accompanying the charge-ordering transition at T_{COI}, whereas no obvious change is observed at T_N. These insights would help clarify the controversy regarding the nature of the phase transitions in various strongly correlated oxides. We also showed the evidence of phase separation at the surface in the *CE* phase regime, where the ferromagnetic phase domains show very high magnetic anisotropy, confirming the ferromagnetic tendency at the surface in the *CE* phase. These results would enrich our understanding of phase separation and spark the interest in exploring unconventional surface states in strongly correlated systems.

METHODS

Magnetic force microscopy
The description of the 20 T MFM and the detailed explanation of the image contrast formation can be found in refs. [37,39]. It uses the frequency-modulated mode to image the stray field from the sample, and the contrast (δf) is proportional to the second derivative of B_z ($\delta f \propto \frac{\partial^2 B_z}{\partial z^2}$). When the magnetic moments of both the tip and sample are all aligned with the external magnetic field, the darker area (with a larger negative δf) is then due to a larger attractive force. The lift height is ~100 nm for all the images. WSxM is used to analyze the MFM images[49].

PCMO film deposition and characterization
The details regarding the deposition and structural characterization of the thin film have been described elsewere[35–37]. The resistivity was measured using a physical property measurement system from Quantum Design. The magnetization was measured in a superconducting quantum interference device from Quantum Design.

Magnetic image simulation
Mumax3[50] is used to perform the micromagnetic simulations presented in this work. As it can simulate MFM images by calculating the same quantity, i.e., the second derivative of B_z on z (z is in the out-of-plane direction)[50], we can compare these simulated images with the measured images directly. We use a grid of $128 \times 128 \times 32$ pixels with an actual size of 1 μm × 1 μm × 32 nm. The domain diameter is 300 nm. The saturation magnetization and exchange stiffness are 6×10^5 A/m and 10^{-12} J/m, respectively. The tip is set as a magnetic dipole. The tip lift height is set to 150 nm as it shows the profile which matches the best with the experiment. The magnetic images of in-plane domains with the thickness of 1, 2, 4, 8, 12, 16, 20, 24, 28, and 32 nm, and out-of-planes with 32 nm thickness have been simulated. The robustness of the simulation can be seen in Supplementary Figures 6 and 7.

DATA AVAILABILITY
The data that support the findings of this study are available from the corresponding authors upon reasonable request.

CODE AVAILABILITY
The Mumax3 codes used in this study are available from the corresponding authors upon reasonable request.

REFERENCES
1. Dagotto, E. Complexity in strongly correlated electronic systems. *Science* **309**, 257–262 (2005).
2. Goodenough, J. B. Theory of the role of covalence in the perovskite-type manganites [La, M(II)]MnO₃. *Phys. Rev.* **100**, 564–573 (1955).
3. Lees, M. R., Barratt, J., Balakrishnan, G., Mc, K. P. D. & Yethiraj, M. Influence of charge and magnetic ordering on the insulator-metal transition in Pr₁₋ₓCaₓMnO₃. *Phys. Rev. B* **52**, 14303–14307 (1995).
4. Tomioka, Y., Asamitsu, A., Kuwahara, H., Moritomo, Y. & Tokura, Y. Magnetic-field-induced metal-insulator phenomena in Pr₁₋ₓCaₓMnO₃ with controlled charge-ordering instability. *Phys. Rev. B* **53**, R1689–R1692 (1996).
5. Daoud-Aladine, A., Rodriguez-Carvajal, J., Pinsard-Gaudart, L., Fernandez-Diaz, M. T. & Revcolevschi, A. Zener polaron ordering in half-doped manganites. *Phys. Rev. Lett.* **89**, 097205 (2002).
6. Tomioka, Y. et al. Magnetic-field-induced metal-insulator transition in perovskite-type manganese oxides. *Phys. B Condens. Matter* **237-238**, 6–10 (1997).
7. Millange, F., Brion, S. D. & Chouteau, G. Charge, orbital, and magnetic order in Nd₀.₅Ca₀.₅MnO₃. *Phys. Rev. B* **62**, 5619–5626 (2000).
8. Moritomo, Y., Tomioka, Y., Asamitsu, A., Tokura, Y. & Matsui, Y. Magnetic and electronic properties in hole-doped manganese oxides with layered structures: La₁₋ₓSr₁₊ₓMnO₄. *Phys. Rev. B* **51**, 3297–3300 (1995).
9. Dagotto, E. Nanoscale phase separation and colossal magnetoresistance: the physics of manganites and related compounds. (Springer Science & Business Media, 2013).
10. van den Brink, J., Khaliullin, G. & Khomskii, D. Charge and orbital order in half-doped manganites. *Phys. Rev. Lett.* **83**, 5118–5121 (1999).
11. Jirák, Z. et al. Magnetism and charge ordering in Pr₀.₅CaₓSr₀.₅₋ₓMnO₃ (x = 0.09 and 0.5). *Phys. Rev. B* **61**, 1181–1188 (2000).
12. Tokunaga, M., Miura, N., Tomioka, Y. & Tokura, Y. High-magnetic-field study of the phase transitions of R₁₋ₓCaₓMnO₃ (R=Pr, Nd). *Phys. Rev. B* **57**, 5259–5264 (1998).
13. Marumoto, K., Soda, K., Kuroda, S.-I. & Moritomo, Y. ESR Studies of Layered-Perovskite Manganites R₀.₅Sr₁.₅MnO₄ (R= La, Nd). *J. Phys. Soc. Jpn.* **72**, 582–587 (2003).
14. Ye, F. et al. Electronically smecticlike liquid-crystal phase in a nearly half-doped manganite. *Phys. Rev. B* **72**, 212404 (2005).
15. Senff, D. et al. Melting of magnetic correlations in charge-orbital ordered La₁/₂Sr₃/₂MnO₄: competition of ferromagnetic and antiferromagnetic states. *Phys. Rev. B* **77**, 184413 (2008).
16. Jooss, C. et al. Polaron melting and ordering as key mechanisms for colossal resistance effects in manganites. *Proc. Natl Acad. Sci. USA* **104**, 13597–13602 (2007).
17. Wu, L., Klie, R. F., Zhu, Y. & Jooss, C. Experimental confirmation of Zener-polaron-type charge and orbital ordering in Pr₁₋ₓCaₓMnO₃. *Phys. Rev. B* **76**, 174210 (2007).
18. Massee, F. et al. Bilayer manganites reveal polarons in the midst of a metallic breakdown. *Nat. Phys.* **7**, 978–982 (2011).
19. Giovannetti, G., Kumar, S., van den Brink, J. & Picozzi, S. Magnetically induced electronic ferroelectricity in half-doped manganites. *Phys. Rev. Lett.* **103**, 037601 (2009).
20. Lopes, A. M. et al. New phase transition in the Pr₁₋ₓCaₓMnO₃ system: evidence for electrical polarization in charge ordered manganites. *Phys. Rev. Lett.* **100**, 155702 (2008).
21. Zou, T., Wang, F., Liu, Y., Yan, L.-Q. & Sun, Y. Multiferroicity and magnetoelectric coupling in half-doped manganite La₀.₅Ca₀.₅MnO₃. *Appl. Phys. Lett.* **97**, 092501 (2010).
22. Garcia-Fernandez, M. et al. Orbital order at Mn and O sites and absence of Zener polaron formation in manganites. *Phys. Rev. Lett.* **103**, 097205 (2009).
23. Grenier, S. et al. Resonant x-ray diffraction of the magnetoresistant perovskite Pr₀.₆Ca₀.₄MnO₃. *Phys. Rev. B* **69**, 134419 (2004).
24. Subias, G. et al. Checkerboard-ordered pattern of Bi₀.₅Sr₀.₅MnO₃ low-temperature phase probed by x-ray resonant scattering. *Phys. Rev. B* **73**, 205107 (2006).
25. Senff, D. et al. Spin-wave dispersion in orbitally ordered La₁/₂Sr₃/₂MnO₄. *Phys. Rev. Lett.* **96**, 257201 (2006).
26. Herrero-Martin, J., Garcia, J., Subias, G., Blasco, J. & Sanchez, M. C. Structural origin of dipole x-ray resonant scattering in the low-temperature phase of Nd₀.₅Sr₀.₅MnO₃. *Phys. Rev. B* **70**, 024408 (2004).
27. Johnstone, G. E., Perring, T. G., Sikora, O., Prabhakaran, D. & Boothroyd, A. T. Ground state in a half-doped manganite distinguished by neutron spectroscopy. *Phys. Rev. Lett.* **109**, 237202 (2012).

28. Ewings, R. A. et al. Spin excitations used to probe the nature of exchange coupling in the magnetically ordered ground state of $Pr_{0.5}Ca_{0.5}MnO_3$. *Phys. Rev. B* **94**, 014405 (2016).

29. Coey, M. Charge-ordering in oxides. *Nature* **430**, 155–157 (2004).

30. Trokiner, A., Yakubovskii, A., Verkhovskii, S., Gerashenko, A. & Khomskii, D. ^{17}O NMR as a conclusive probe of charge-ordering models in half-doped manganites. *Phys. Rev. B* **74**, 092403 (2006).

31. Rao, S. S. & Bhat, S. V. Probing the existing magnetic phases in $Pr_{0.5}Ca_{0.5}MnO_3$ (PCMO) nanowires and nanoparticles: magnetization and magneto-transport investigations. *J. Phys. Condens. Matter* **22**, 116004 (2010).

32. Zhang, T., Wang, X. P. & Fang, Q. F. Exchange bias effect and suppression of charge ordering induced by a surface phase separation in $La_{0.25}Ca_{0.75}MnO_3$ nanowires. *J. Phys. Chem. C* **114**, 11796–11800 (2010).

33. Dong, S., Yu, R., Yunoki, S., Liu, J. M. & Dagotto, E. Ferromagnetic tendency at the surface of CE-type charge-ordered manganites. *Phys. Rev. B* **78**, 064414 (2008).

34. Valencia, S. et al. Enhancement of spin-orbit coupling at manganite surfaces. *Phys. Rev. B* **98**, 115142 (2018).

35. Okuyama, D. et al. Epitaxial-strain effect on charge/orbital order in $Pr_{0.5}Ca_{0.5}MnO_3$ films. *Appl. Phys. Lett.* **95**, 152502 (2009).

36. Wadati, H. et al. Revealing orbital and magnetic phase transitions in $Pr_{0.5}Ca_{0.5}MnO_3$ epitaxial thin films by resonant soft x-ray scattering. *N. J. Phys.* **16**, 033006 (2014).

37. Sheng, Z. et al. Visualization of electronic multiple ordering and its dynamics in high magnetic field: evidence of electronic multiple ordering crystals. *ACS Appl. Mater. Interfaces* **10**, 20136–20141 (2018).

38. Zhou, H., Wang, Z., Hou, Y. & Lu, Q. A compact high field magnetic force microscope. *Ultramicroscopy* **147**, 133–136 (2014).

39. Zhou, H. et al. Evolution and control of the phase competition morphology in a manganite film. *Nat. Commun.* **6**, 8980 (2015).

40. Israel, C., Wu, W. & Lozanne, A. D. High-field magnetic force microscopy as susceptibility imaging. *Appl. Phys. Lett.* **89**, 032502 (2006).

41. Wang, Z.-H., Lebedev, O. I., Van Tendeloo, G., Cristiani, G. & Habermeier, H. U. Crosshatching on $La_{0.5}Ca_{0.5}MnO_3$ ultrathin films epitaxially grown on $SrTiO_3$(100). *Phys. Rev. B* **77**, 115330 (2008).

42. Solovyev, I. V. Charge ordering due to magnetic symmetry breaking. *Phys. Rev. Lett.* **91**, 177201 (2003).

43. Bao, W., Axe, J. D., Chen, C. H. & Cheong, S. W. Impact of charge ordering on magnetic correlations in perovskite (Bi,Ca)MnO_3. *Phys. Rev. Lett.* **78**, 543–546 (1997).

44. Chen, C. H., Cheong, S. W. & Cooper, A. S. Charge modulations in $La_{2-x}Sr_xNiO_{4+y}$: ordering of polarons. *Phys. Rev. Lett.* **71**, 2461–2464 (1993).

45. Meiklejohn, W. H. & Bean, C. P. New magnetic anisotropy. *Phys. Rev.* **105**, 904–913 (1957).

46. Giri, S. K., Yusuf, S. M., Mukadam, M. D. & Nath, T. K. Enhanced exchange bias effect in size modulated $Sm_{0.5}Ca_{0.5}MnO_3$ phase separated manganite. *J. Appl. Phys.* **115**, 093906 (2014).

47. Stamps, R. L. Mechanisms for exchange bias. *J. Phys. D.* **33**, R247–R268 (2000).

48. Lai, K. et al. Mesoscopic percolating resistance network in a strained manganite thin film. *Science* **329**, 190–193 (2010).

49. Horcas, I. et al. WSXM: a software for scanning probe microscopy and a tool for nanotechnology. *Rev. Sci. Instrum.* **78**, 013705 (2007).

50. Vansteenkiste, A. et al. The design and verification of MuMax3. *AIP Adv.* **4**, 107133 (2014).

AUTHOR CONTRIBUTIONS

H.Z., Z.S., and Q.L. conceived the project. H.Z. and Q.F. conducted the MFM measurements with assistance from Y.H. Z.S. made the sample and measured the transport with the help of M.N., Y.T., and M.K. Q.F. performed the magnetization measurement. H.Z. performed the micromagnetic simulation. H.Z., Z.S., and Q.L. analyzed the data. H.Z. wrote the manuscript under the supervision of Z.S. and Q.L. with input from all the other authors.

COMPETING INTERESTS

The authors declare no competing interests.

ADDITIONAL INFORMATION

Supplementary information The online version contains supplementary material available at https://doi.org/10.1038/s41535-021-00353-2.

Correspondence and requests for materials should be addressed to H.Z., Z.S. or Q.L.

Reprints and permission information is available at http://www.nature.com/reprints

Publisher's note Springer Nature remains neutral with regard to jurisdictional claims in published maps and institutional affiliations.